PERGAMON

Deep-Sea Research II 49 (2002) 1423–1439

DEEP-SEA RESEARCH
PART II

www.elsevier.com/locate/dsr2

The overflows across the Ninetyeast Ridge

Bruce A. Warren[a,*], Gregory C. Johnson[b]

[a] *Physical Oceanography Department, Woods Hole Oceanographic Institution, Clark 325A, MS 21, Woods Hole, MA 02543, USA*
[b] *Pacific Marine Environmental Laboratory, NOAA, Seattle, WA 98115, USA*

Accepted 20 September 2001

Abstract

Water deeper than, say, 3800 m in the Central Indian Basin comes from the West Australian Basin across deep saddles on the Ninetyeast Ridge near Lats. 5°S, 10°S, and 28°S. The WOCE Hydrographic Program in the Indian Ocean (1994–1996) provided opportunities for more detailed measurements of water properties in these overflows than any made earlier. With zero-velocity surfaces inferred from contrasts in oxygen and silicic-acid concentrations and from distributions of specific-volume anomaly, geostrophic estimates of these overflow rates are, respectively, 1.0, 1.1, and 0.1×10^6 m^3 s^{-1} (westward). These constructions also imply strong zonal flows of mid-depth water (between 2000 db and the zero-velocity surfaces) through the passages: 2.2 and 6.7×10^6 m^3 s^{-1} *westward* at Lats. 5°S and 10°S, respectively, and 1.8×10^6 m^3 s^{-1} *eastward* at Lat. 28°S. As in the southward flow through Denmark Strait, density stratification explains the splitting of westward currents at 5°S and 10°S into mid-depth and deep flows as they pass over their saddles (but not why such vertically extended flows should exist in the first place). The cause of opposed eastward flow at 28°S is less certain, but might be related to the particular geometry of the West Australian Basin.

1. Introduction

Deep water in the Central Indian Basin is Circumpolar Deep Water from the South Australia Basin (Fig. 1a). It enters the Central Basin (Fig. 1b) by two routes (e.g., Toole and Warren, 1993). Water flowing northwestward toward the junction between the Southeast Indian Ridge and the Ninetyeast Ridge near 33°S, 85°E splits, that above isobaths shallower than the sill depth of the saddle (between 3500 and 4000 m, according to Fisher et al., 1982) continuing northwestward along the eastern flank of the Southeast Indian Ridge as a western-boundary current marked by high oxygen and low silicic acid. This current supplies the upper deep water (shallower, say, than 3800 m) in the Central Basin. The water flowing above the deeper isobaths in the South Australia Basin turns eastward along the Broken Plateau and enters the Perth Basin. It proceeds northward as another boundary current, probably to the northern limit of the East Indiaman Ridge (Fig. 1a), and turns westward to feed the deep western-boundary-current system of the West Australian Basin, along the Ninetyeast Ridge. (The physically sensible idea of a zonal jet at the north end of the East Indiaman Ridge is substantiated in a deep front evident in the nutrient

*Corresponding author. Tel.: +1-508-289-2537; fax: +1-508-457-2181.
E-mail address: bwarren@whoi.edu (B.A. Warren).

0967-0645/02/$ - see front matter
PII: S0967-0645(01)00156-4

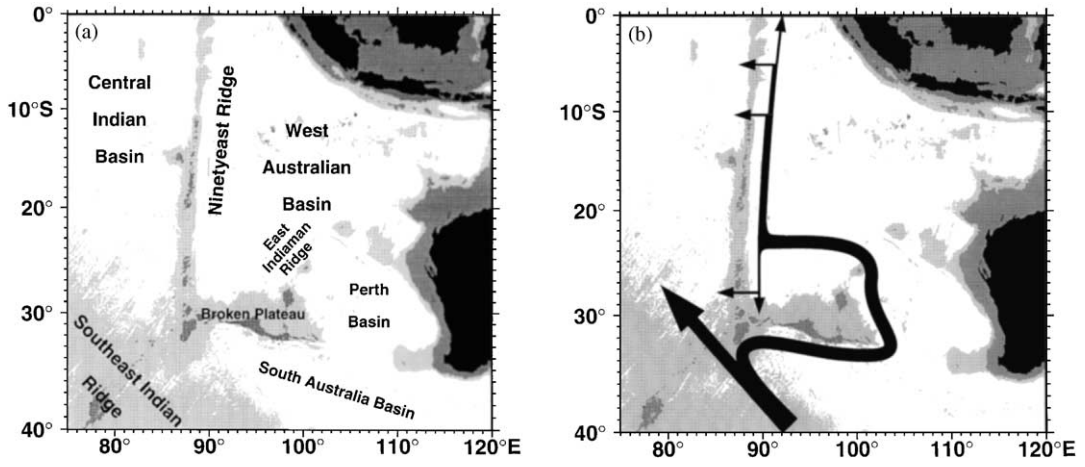

Fig. 1. (a) Index map of the eastern South Indian Ocean identifying names of geographical features. Shading indicates isobaths of 2000 and 4000 m from GTOPO 30 (Smith and Sandwell, 1997; available at http://edcwww.cr.usgs.gov/landdac/gtopo30/gtopo30.html). (b) Index map of the eastern South Indian Ocean showing schematic course of deep boundary currents and locations of deep overflows across the Ninetyeast Ridge supplying lower deep water to the Central Indian Basin. Bathymetry as in (a).

fields near Lat. 24°N on the WOCE section I9N along Long. 95°E; the as yet unpublished data are available at http://whpo.ucsd.edu/data/onetime/indian/io9/io9n/index.htm.) Some of that water in turn spills over deep saddles on the Ninetyeast Ridge to form the colder, oxygen-richer, lower deep water of the Central Basin.

South of the equator there are four saddles deeper than 3000 m: near Lats. 3°S, 5°S, 10°S, and 28°S; overflows have been found at the last three (Fig. 1b). Reconnaissance for them was first done in 1979 on a hydrographic section occupied along the western flank of the Ninetyeast Ridge from Lat. 12°S to Lat. 1°N (Warren, 1982). A meridional density jump, combined with anomalously cold, oxygen-rich water at a single station, disclosed one overflow at the 10°S saddle; a slight density jump suggested another, weaker one at the 5°S saddle. Closely spaced stations proved that there was none at 3°S. Because of anomalously cold bottom water found later in the southeastern corner of the Central Basin, Toole and Warren (1993) conjectured that there was a third overflow at the 28°S saddle. Therefore, during the I8N cruise leg of the US WOCE Indian Ocean Expedition on the R.V. *Knorr* (1994–1996), McCarthy et al. (1997) surveyed that area in detail, and discovered that overflow.

The Indian Ocean Expedition also afforded an opportunity (cruise leg I2) to delineate and measure the 10°S and 5°S overflows with more detailed and more extensive coverage by hydrographic stations than had been possible on the reconnaissance cruise 17 years earlier. The purpose of this paper is to describe results concerning those two overflows, and to combine them with an analysis of data from the 28°S saddle to make a gross estimate of the deep inflow to the Central Indian Basin across the Ninetyeast Ridge. (It is possible that there is some inflow as well around the northern end of the ridge at a low point near Lat. 10°N, but water-property data that we have examined are complicated, limited in scope, and amenable to contrary interpretations; they make it unlikely, though, that such a flow could be substantial in comparison to the overflows at Lats. 5°S and 10°S.)

Hydrographic stations were made with a Mark-III EG&G conductivity–temperature–pressure microprofiler (CTD) equipped with a Beckman polarographic dissolved-oxygen sensor and a General Oceanics rosette sampler bearing 36 10-l Niskin bottles. Samples were drawn from the Niskin bottles for analysis of salinity and dissolved-oxygen concentration to calibrate the CTD sensors, and for analysis of nutrients and many

other chemical constituents. Water properties treated here, however, are only temperature, salinity, oxygen, and silicic acid. The respective measurement accuracies are considered to be 0.001°C, 0.001, and 0.02 ml l^{-1} for the calibrated CTD records, and 1% for silicic acid. Standard Seawater batch P128 was used on cruise leg I2. The CTD stations on the I2 and I8N cruise legs were done by the Woods Hole Oceanographic Institution CTD Group, and by the Oceanographic Data Facility of the Scripps Institution of Oceanography, respectively. Nutrient analyses were performed with a Technicon AutoAnalyzer II, by personnel from Oregon State University on leg I2, and by Scripps personnel on leg I8N; the methods used are described by Gordon et al. (1994). Hydrographic data from the WOCE Indian Ocean Expedition are available at the WOCE Hydrographic Program Office at the Scripps Institution of Oceanography.

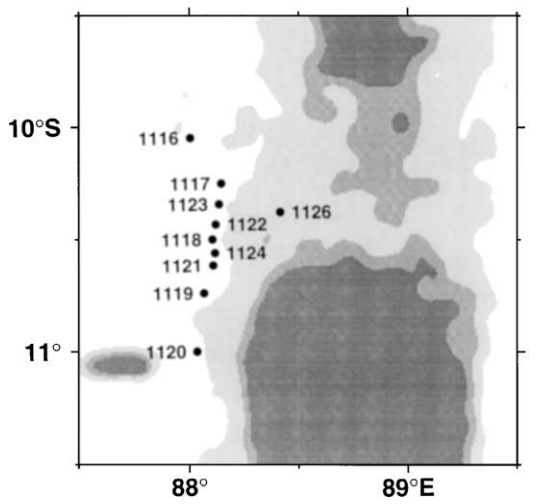

Fig. 2. Bottom topography in vicinity of 10°S saddle, including positions of WHP Stas. 1116–1124 and 1126 (17–19 December 1995). Shading denotes isobaths of 3500, 3900, and 4500 m from GTOPO 30.

2. The overflow at 10°S

US WOCE Indian Ocean Stations Stas. 1116–1124 were occupied in a broken line along the western flank of the Ninetyeast Ridge, near its base, to form a section fronting the 10°S saddle and crossing the overflow; Sta. 1126 was made higher on the ridge, in water depth of about 4100 m, closer to the actual saddle (Fig. 2). The GEBCO bathymetry (Fisher et al., 1982) puts the sill depth between 3500 and 4000 m; the more recent GTOPO 30 specifies it as between 3900 and 4000 m. The GTOPO 30 data set relies upon shipboard bathymetric measurements to calibrate satellite gravity-anomaly data through a spectral transfer function, and rms errors of 250 m are likely in areas of steep topography with little bathymetric control (Smith and Sandwell, 1997). This uncertainty applies here, as well as to all other citations of GTOPO 30 sill depths below.

To help interpret the distributions of oxygen and silicic-acid concentrations along the section, the deep-water correlations between these properties and potential temperature are contrasted across the Ninetyeast Ridge in Fig. 3, from stations made on the WOCE transindian section I2, here running along Lat. 8°S. In the temperature interval 1.0–1.4°C, the water in the Central Basin is measurably poorer in oxygen and richer in silicic-acid concentration than that in the West Australian Basin east of the ridge. Below 1.0°C, the waters are virtually identical (the bottom water of the Central Basin being overflow-derived), except that the West Australian Basin water reaches lower temperatures, with higher oxygen and lower silicic-acid concentrations. Above 1.4°C, the oxygen–temperature relations are the same, but the Central Basin water is lower in silicic acid. With respect to absolute values, the oxygen concentrations are likely to be slightly lower, the silicic-acid concentrations slightly greater, than at the more southerly latitude of the deep saddle.

According to the distribution of potential temperature along the section (Fig. 4a), below about 3900 m isotherms slope upward to the south, indicating zonal geostrophic flow becoming more westward (or less eastward) with depth, while above about 3700 m they slope downward to the south, marking the geostrophic flow as becoming more westward with elevation. A minimum potential temperature of 0.89°C was found at the bottom at Stas. 1122 and 1123, to be compared

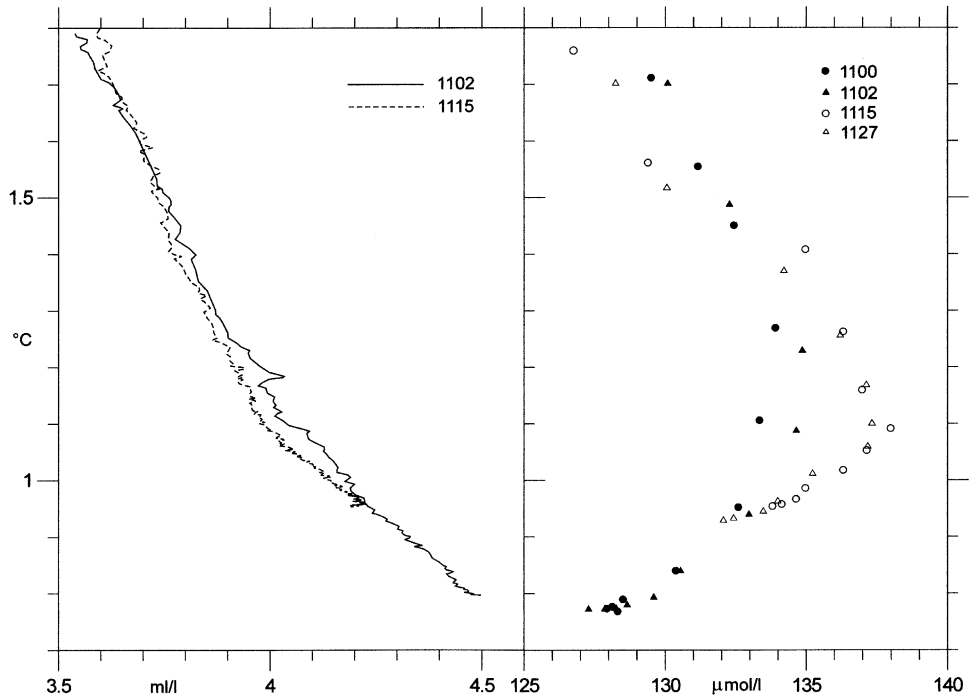

Fig. 3. Plots vs. potential temperature (ordinate, °C) of dissolved-oxygen correlation (left, ml l^{-1}) and silicic-acid concentration (right, µmol l^{-1}) for WOCE stations at Lat. 8°S just east (Stas. 1100 and 1102; 12–13 December 1995) and just west (Stas. 1115 and 1127; 16 and 19 December 1995) of the Ninetyeast Ridge. Longitudes for the stations are: 1100, 91°20′E; 1102, 90°00′E; 1115, 88°00′E; and 1127, 87°20′E.

to typical very deep temperatures in the Central Indian Basin of 0.9–1.1°C (Warren, 1982, Fig. 19; Mantyla and Reid, 1995, Fig. 2b). The bottom temperature at Sta. 1126 (depth 4109 m), closer to the sill for the overflow, was lower yet, 0.83°C, like that observed (0.82°C, depth 4300 m) near the sill on the 1979 reconnaissance section (Warren, 1982). (On the *eastern* flank of the ridge, at Lat. 18°S, water of this temperature was found at about 3800 m (Warren, 1981).) This most extreme West Australian Basin water occurred on the section as thin, cold bottom layers at Stas. 1117, 1123, 1122, and 1118, directly fronting the deepest point in the saddle (Fig. 2). The step structures at Stas. 1117 and 1122 (Fig. 5) bound those at Stas. 1123 and 1118, and the step at Sta. 1126 (Fig. 5), up on the ridge, was much more pronounced. Cold bottom water centered near Lat. 10°S along Long. 80°E (Talley and Baringer, 1997, Fig. 1b) registers the westward jet of overflow water from this site (and probably that at Lat. 5°S as well) predicted by simple circulation theory (Warren, 1982).

The salinity varies by little more than 0.01 below 3000 m in the Central Basin (Fig. 4b, but true basinwide). This is very slight: a change of that amount at 3000 m, say, is equivalent in its effect on density to a temperature change of merely 0.05°C.

Oxygen isopleths (Fig. 4c) from 3.00 to 3.75 ml l^{-1} parallel the potential isotherms, and are therefore uninformative, but the doming of the 4.00-isopleth in the station interval 1123–1119 represents enrichment of oxygen on local isotherms (about 1.0–1.3°C), and marks inflow of water from the oxygen-richer environment east of the Ninetyeast Ridge (Fig. 3). The southward increase in oxygen concentration below 4300 m accompanied by decrease in temperature, is consistent with the expected deep poleward interior movement carrying overflow water southward

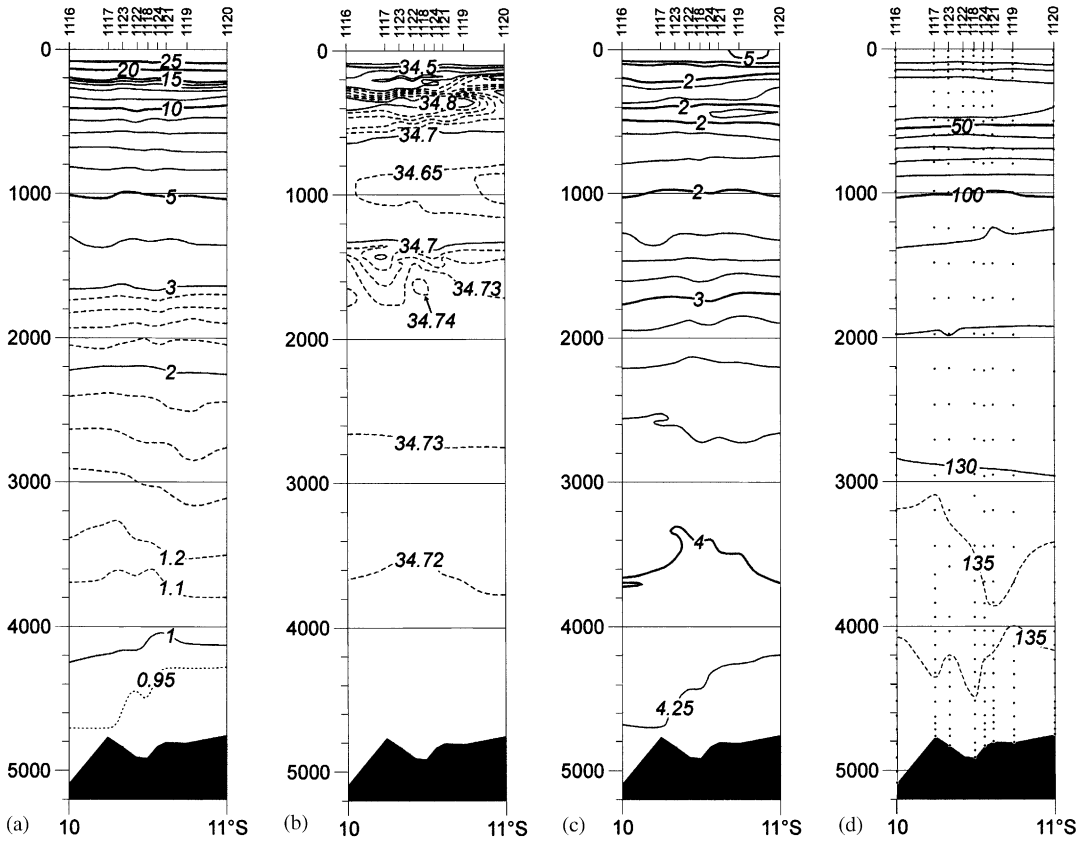

Fig. 4. Profiles of potential temperature (a, °C), salinity (b), dissolved-oxygen concentration (c, ml l^{-1}), and silicic-acid concentration (d, μmol l^{-1}) for section facing 10°S saddle. Dots indicate positions of water samples. Station numbers along top, latitude along bottom. Depth in meters. See Fig. 2 for station locations.

(Warren, 1982). The maximum oxygen concentration observed at the bottom here, 4.40 ml l^{-1} on Sta. 1122, is distinctly less than the 4.49 ml l^{-1} at Sta. 1126 higher on the ridge. (The maximum value on the reconnaissance section was 4.53 ml l^{-1}.)

The deep maximum in silicic-acid concentration (Fig. 4d) is diminished sharply at Stas. 1119, 1121, and 1124. That reduction is another marker of water from the eastern side of the Ninetyeast Ridge (Fig. 3). The minimum bottom concentration, 131 μmol l^{-1} at Sta. 1122, is again less extreme than at Sta. 1126 (130 μmol l^{-1}), but for this property, in contrast to oxygen, the difference is within observational error.

Plots of oxygen and silicic-acid concentrations against potential temperature reveal further qualitative aspects of the flow field. Three characteristic stations are illustrated in Fig. 6. The curves for Sta. 1117 are similar to those for the adjacent northernmost station, 1116, as well as the southernmost station, 1120; they match the pure Central Basin water of Fig. 3. The curves for Sta. 1124 resemble those for the stations immediately to the south, 1121 and 1119. Those for the adjacent stations, 1122 and 1118, lie between those for the bracketing stations, 1123 and 1124.

The group 1124, 1121, and 1119 show relatively pure West Australian Basin water (Fig. 3) down to about 1.06°C, below which the curves shift to Central Basin water in a narrow temperature interval, before registering the overflow-derived bottom water colder than around 1.0°C. The thin Central Basin layer is especially well defined at Sta.

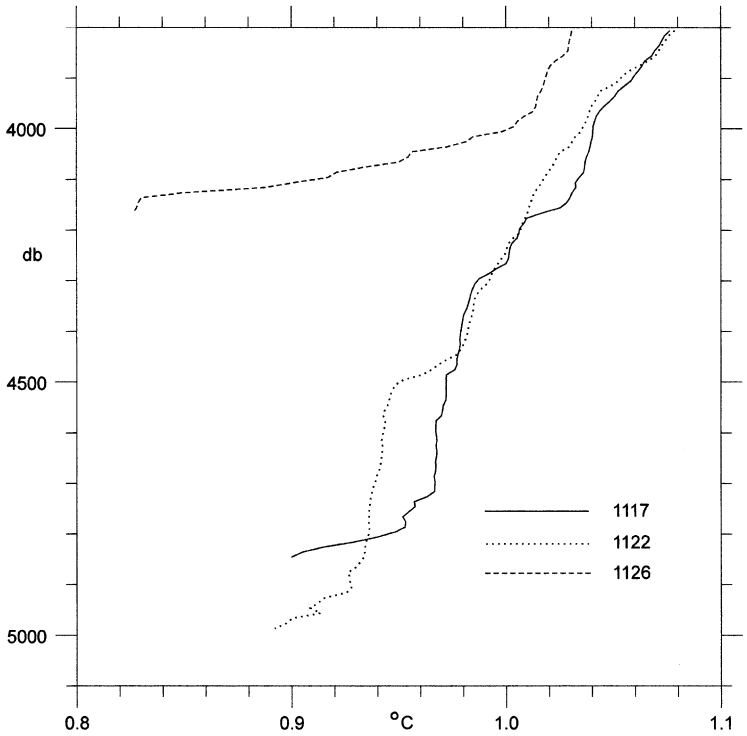

Fig. 5. Potential temperature (°C) vs. pressure (db) below 3800 db at Stas. 1117 and 1122 on section facing 10°S saddle, and at Sta. 1126 on the saddle. See Figs. 2 and 4 for station locations.

1124 by the sharp silicic-acid maximum, nearly 137 μmol l^{-1} (Fig. 6), contrasting with the lesser maxima in the West Australian Basin of 134−135 μmol l^{-1} (Fig. 3); the corresponding oxygen minimum is consistent, though not decisive in itself. However, on Sta. 1123, next to the northern stations of pure Central Basin characteristics, the West Australian Basin water occurs only down to about 1.18°C before being displaced by Central Basin water below 1.15°C. The intervening stations also show a jump from one water type to the other, but at intermediate temperatures.

Thus, the combined evidence of cold bottom steps and of oxygen and silica contrasts identifies the inflow from the West Australian Basin as occurring between Stas. 1117 and 1119. It occurs, moreover, in two layers: one above a depth ranging from around 3400 to 3800 m (top of the layer not indicated), and the other below roughly 4200 m, with Central Basin water in between. On a reduced scale, this structure resembles that of the outflow from the Greenland Sea through the Denmark Strait. There the flow is southward, sea surface to bottom, close to Greenland in the strait. As the outflow proceeds into deep water, its upper part, carrying water of similar density to that farther south, continues as an upper-ocean western-boundary current, the East Greenland Current; but the deeper part of the outflow, which carries water denser than any in the open Atlantic, plunges to depth, entraining ambient water as it goes, to become the overflow current. Thus, the outflow is split vertically, with mostly ambient Atlantic water interposed between the resulting two currents, and the remaining Greenland Sea water in that interval stretched so much as to have little residual forward motion (Warren and Owens, 1988; Spall and Price, 1998). Swallow and Worthington (1969) even thought it practical to invoke a level-of-no-motion between these two currents at the southern tip of Greenland for doing geostrophic calculations.

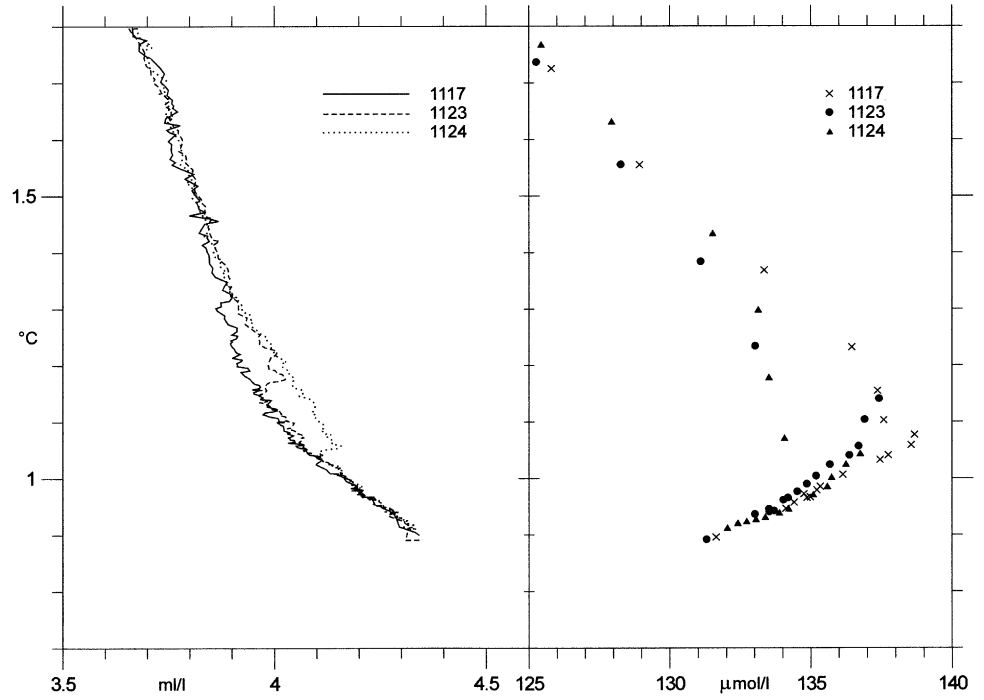

Fig. 6. Plots vs. potential temperature (°C) of dissolved-oxygen concentration (left, ml l^{-1}) and silicic-acid concentration (right, µmol l^{-1}) at characteristic stations 1117, 1123, and 1124 on section facing 10°S saddle. See Figs. 2 and 4 for station locations.

The deep westward inflow to the Central Basin across the 10°S saddle appears to be split in a similar fashion, and perhaps a zero-velocity surface also may be usefully construed within the inserted layer of Central Basin water. Water within the inserted layer can hardly be moving westward (from the West Australian Basin); while the layer is as prominent in property plots at Sta. 1126, up on the Ninetyeast Ridge (Fig. 2), as at Sta. 1124 (Fig. 6), Central Basin water has not been detected in the West Australian Basin (to match the West Australian Basin water found in the very deep Central Basin), so it is unlikely that there is much eastward movement in this layer either. Thus, zero zonal velocity seems a plausible inference within the inserted layer.

The distribution of horizontal density difference is consistent with this surmise. The extreme differences are for the curves of specific-volume anomaly vs. pressure at the ends of the section (Fig. 7, Stas. 1116 and 1120). They cross near 4000 m, with horizontally integrated geostrophic shears above and below as suggested by the temperature profile (Fig. 4a). The curve for a sample intervening station, 1124, lies between these two, but crosses them at different depths, still within the temperature interval of the Central Basin layer, as do the curves for the other intervening stations. This behavior implies a zero-velocity surface of varying depth, if the depths of zero shear for successive station pairs correspond to depths of zero velocity.

From consideration of the oxygen and silicic-acid tracer features discussed above, and the characteristics of the specific-volume-anomaly field, we propose the following zero-velocity surface for geostrophic calculations: 4000 db for station pairs 1116–1117, 1117–1123, 1124–1121, 1121–1119, and 1119–1120; 3800 db for 1122–1118 and 1118–1124; and 3900 db for 1123–1122. For estimating transport through the "bottom triangle" below the deepest common level of a station pair, we have taken the speed to be that at the deepest common level. The geostrophic transport

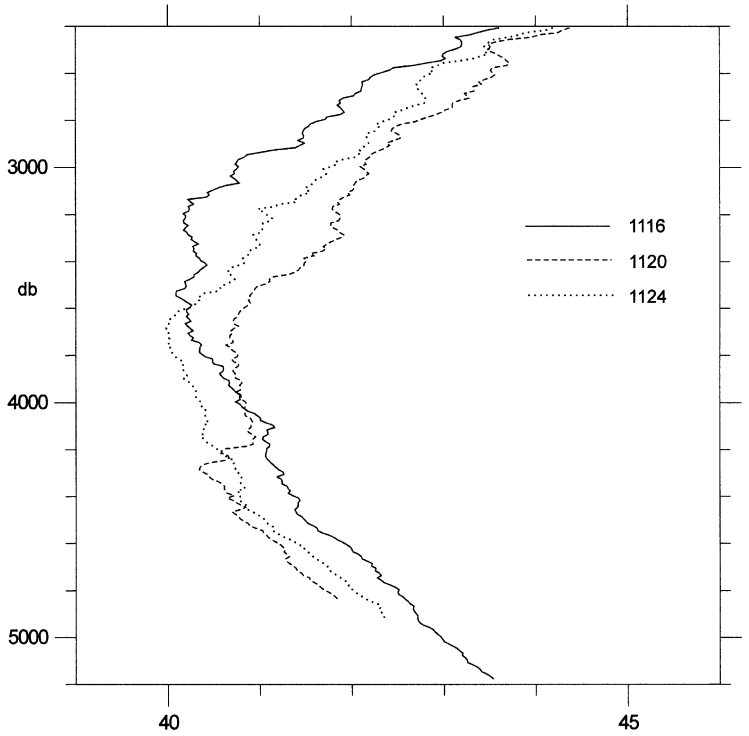

Fig. 7. Specific-volume anomaly (10^{-5} cm^3 g^{-1} or 10^{-8} m^3 kg^{-1} or cl ton^{-1}) vs. pressure (db) at three stations on section facing 10°S saddle. See Figs. 2 and 4 for station locations.

below the zero-velocity surface is then 1.1×10^6 m^3 s^{-1} westward, and that above it, to the 2000-db pressure, is 6.7×10^6 m^3 s^{-1}, also westward. (2000 db is a purely arbitrary "top" for the deep water, and is introduced as an upper limit here and in the subsequent calculations for relative comparisons of flows above and below zero-velocity surfaces, and between the different passages.) The maximum calculated speed (velocity component normal to the section) below the zero-velocity surface was 7.8 cm s^{-1}, at the bottom between Stats. 1124 and 1121. The "bottom triangle" increment amounted to only 0.1×10^6 m^3 s^{-1}.

Given the distribution of specific-volume anomaly, moving the zero-velocity surface up or down by 100 m would have little effect on the calculated transports. However, the calibrated salinity records are thought accurate to about 0.001, equivalent to an uncertainty in deep specific-volume anomaly of 7×10^{-7} cm^3 g^{-1}. In the transport calculation, the end-station difference in specific-volume anomaly is about 6×10^{-6} cm^3 g^{-1} below the zero-velocity surface and about 10×10^{-6} cm^3 g^{-1} above it (Fig. 7), so even such a minute salinity discrepancy between the end stations as 0.001 would produce calculation errors of 12% and 7%, respectively. (The corresponding error in specific-volume anomaly due to temperature error of 0.001°C is $<2 \times 10^{-7}$ cm^3 g^{-1}.)

One can gain some idea of the amount of entrainment into the overflow as it descends the ridge flank by comparing bottom values of properties at Sta. 1126 (Fig. 2), high on the ridge (bottom depth 4109 m), to those at Sta. 1123 (bottom depth 4833 m), a station of extreme bottom-water characteristics on the section (Fig. 6), and then supposing that the difference was achieved by entraining into the former ambient water having the vertically averaged

property values for this depth interval from Sta. 1115, just west of the ridge at Lat. 8°S (Fig. 3). For these three stations, the respective potential-temperature values are 0.827°C, 0.892°C, and 0.986°C; the oxygen values are 4.49, 4.37, and 4.17 ml l^{-1}; and the silicic-acid values are 129.7, 131.3, and 135.2 μmol l^{-1}. For the temperature, oxygen, and silicic-acid values, the calculated fractions α of entrained water at Sta. 1123 are then 0.41, 0.38, and 0.29, respectively, where the last is the least reliable because of silicic-acid uncertainty.

These must be underestimates of the full entrainment into the overflow because the water at Sta. 1126 has already left the sill (Fig. 2), while the water at the section is still on the lower ridge flank and has not yet reached the floor of the basin (depth roughly 5200 m). Moreover, the bottom water in the overflow must have experienced the minimal entrainment since the entrained water enters the overflow from above and from the sides; and Sta. 1123 itself was chosen for its extreme, most clear-cut overflow characteristics (for example, if Sta. 1120, at the southern end of the section, is used instead, the resulting respective values of α increase to 0.48, 0.44, and 0.36). The problem of calculating entrainment from a triad of values for a water property is not well posed, on account of arbitrariness in specifying the property inputs, and estimates are correspondingly imprecise—as illustrated by comparing these calculations to Warren's (1982) values half again as large for the same overflow, but obtained with different definitions and data.

An alternate approach to gauging the entrainment is to subtract the volume transport estimated for the overflow at the 1979 meridional reconnaissance section just west of Sta. 1126 (0.4×10^6 m^3 s^{-1}; Warren, 1982) from that at the WOCE section. The difference, 0.7×10^6 m^3 s^{-1}, implies a value for α of 0.64. The agreement with the water-property results is not very good, but, as argued above, these should probably be regarded as lower-limit estimates; all these calculations at least demonstrate an entrainment that is neither trifling nor overwhelming, and is in line with those observed in other deep, dense, downslope currents (Price and Baringer, 1994).

3. The overflow at 5°S

Stas. 1106–1112 form a section parallel to the Ninetyeast Ridge along the base of its western flank, facing the deep saddle at Lat. 5°S (Fig. 8). The sill depth, according to GEBCO (Fisher et al., 1982), is between 3500 and 4000 m, and GTOPO 30 (Smith and Sandwell, 1997) puts it more precisely at 3900–4000 m, with the sill at 5°30′S, 89°00′E, directly fronting Sta. 1110.

Water-property contrasts are not so pronounced as at 10°S. The bottom water is warmer (Fig. 9a), with minimum bottom potential temperature of 0.92°C at Sta. 1108, and no cold bottom steps in the temperature–depth curves. The deep salinity field (Fig. 9b) is again nearly uniform, and the oxygen distribution (Fig. 9c) follows that of potential temperature, with maximum bottom concentration of 4.28 ml l^{-1} at Sta. 1108. These extreme values are extrema along the section simply because they are the deepest observations there; but they are in fact slightly more extreme than any found at the even deeper stations immediately adjacent to the ridge on the I2 section just to the south (Stas. 1114 and 1115; Lat. 8°00′S;

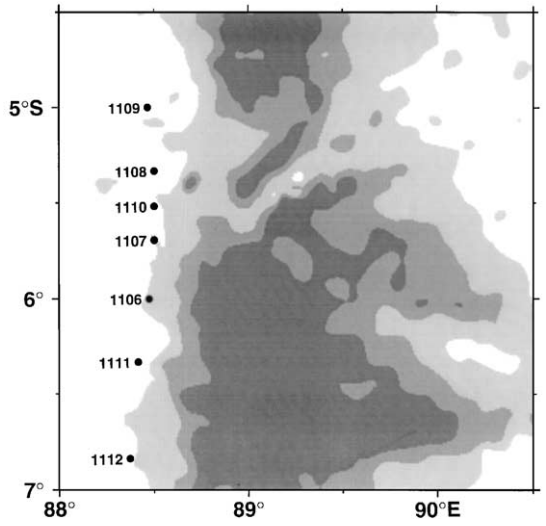

Fig. 8. Bottom topography in vicinity of 5°S saddle, including positions of Stas. 1106–1112 (14–15 December 1995) forming section facing saddle. Shading denotes isobaths of 3500, 3900, and 4500 m from GTOPO 30.

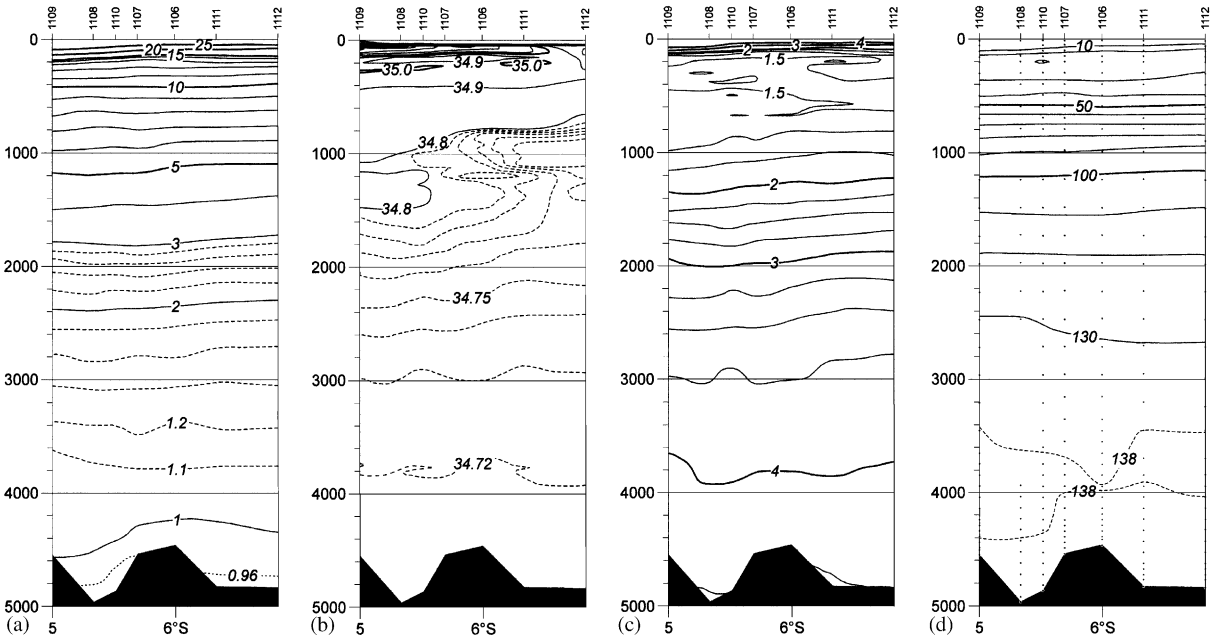

Fig. 9. Profiles of potential temperature (a, °C), salinity (b), dissolved-oxygen concentration (c,ml l^{-1}), and silicic-acid concentration (d, μmol l^{-1}) for section facing 5°S saddle. Dots indicate positions of water samples. Station numbers along top, latitude along bottom. Depth in meters. See Fig. 2 for station locations.

Longs. 88°20′S and 88°00′S, respectively), so they do demonstrate some westward overflow of bottom water at the saddle. Only the silicic-acid field (Fig. 9d) gives clear markers for the sort of two-layer overflow seen at 10°S: the sharp reduction and thinning of the deep maximum at Sta. 1106 registers greater amounts of West Australian Basin water (relatively poor in silicic acid) above about 3800 m and below about 4200 m, with Central Basin water again interposed between.

The thermal-wind shear supports this interpretation of water properties. The curves of specific-volume anomaly vs. pressure for Stas. 1109 and 1112 (Fig. 10), at the northern and southern ends of the section, respectively, cross near 4000 db, so that with a zero-velocity surface at that pressure, the two layers of reduced silicic-acid concentration above and below it should both flow westward from the West Australian Basin. Sta. 1109 reaches only as deep as 4600 db, but the curve for the neighboring Sta. 1108 (Fig. 10) shows that this net thermal wind for the section maintains the same sign from 4600 to 5000 db.

Using 4000 db as the zero-velocity surface, as suggested by the fields of both silicic acid and specific-volume anomaly, produces geostrophic volume transports for the section of 1.0×10^6 m^3 s^{-1} westward below 4000 db, and 2.2×10^6 m^3 s^{-1} westward between 4000 and 2000 db. The "bottom triangle" calculation contributed 0.3×10^6 m^3 s^{-1} to the former, due about half to the large areas of the triangles in the station intervals 1110–1107 and 1106–1111, and about half to the large bottom speed (7.1 cm s^{-1}, the maximum in the overflow) in the interval 1108–1110. Obviously (Fig. 10), moving the zero-velocity surface up or down 100 db would have little effect on the calculated transports, but a different treatment of the bottom triangles (such as extrapolation of constant vertical shear instead of constant velocity) might alter the lower transport noticeably. Moreover, since the end-station difference in specific-volume anomaly is only about 4×10^{-6} cm^3 g^{-1} below 4000 m (Fig. 10), salinity error of 0.001 would throw the lower-transport calculation off by nearly 20%.

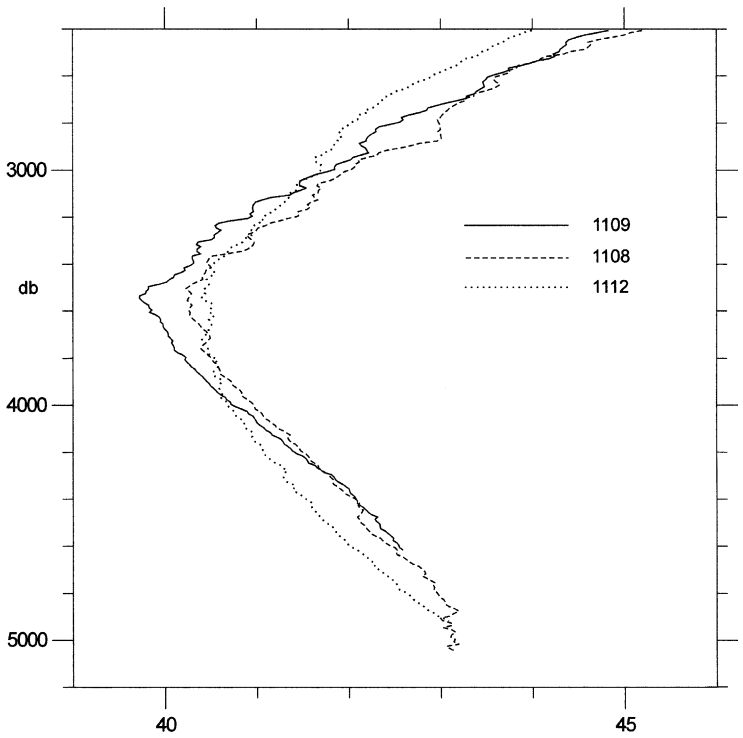

Fig. 10. Specific-volume anomaly (10^{-5} cm^3 g^{-1} or 10^{-8} m^3 kg^{-1} or cl ton^{-1}) vs. pressure (db) for northernmost stations (1109 and 1108) and southernmost station (1112) on section facing 5°S saddle. See Fig. 8 for station locations.

4. The overflow at 28°S

McCarthy et al. (1997) analyzed three roughly meridional sections made in the vicinity of the deep passage near Lat. 28°S: along the eastern flank of the Ninetyeast Ridge, along the center of the ridge, and in the Central Basin just west of the ridge. We limit our analysis to the deep portion of the center transect, Stas. 387–391, the positions of which are included in Fig. 11, but we also compare properties to those at Stas. 363 and 156, the former from the western section, the latter from the earlier I9N cruise leg (Fig. 11).

Little bathymetric control in this region was available to Fisher et al. (1982) for drawing the GEBCO map, which gives the sill depth for the passage as between 3000 and 3500 m. The detailed bathymetry measured by McCarthy et al. (1997) along their cruise track was quite different from the GEBCO interpolation, but rather like GTOPO 30 (Smith and Sandwell, 1997). The latter specifies the sill depth to be between 3500 and 3600 m, as established by two short saddles east of the center transect (Fig. 11; but see below).

Since McCarthy et al. (1997) presented profiles of potential temperature, salinity, and dissolved-oxygen concentration for all their sections, we do not include any water-property profiles here. They estimated geostrophic transports through the central section by assuming zero velocity near 1650 m. We take a different approach, based on a close examination of water-property contrasts.

Plots of the concentration of dissolved oxygen against potential temperature are compared in Fig. 12 for three sample stations: Sta. 363, in the Central Indian Basin off the western side of the Ninetyeast Ridge just north of the 28°S passage; Sta. 390, in the passage itself; and Sta. 156 (from the I9N cruise leg) just north of the Broken Plateau in the West Australian Basin (see Fig. 11 for station positions). In the temperature interval 1.15–1.9°C, the Central Basin water (Sta. 363) is

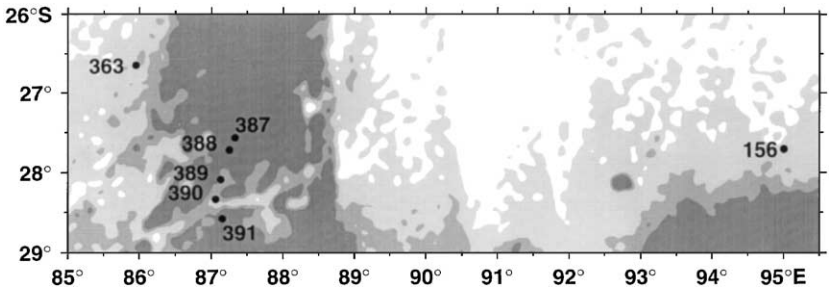

Fig. 11. Bottom topography in vicinity of deep passage near 28°S, including the positions of Stas. 387–391 (2–3 April 1995) which form a section crossing the center of the passage, and of Stas. 363 (29 March 1995) and 156 (29 January 1995), near the western and eastern ends of the passage, respectively. Shading denotes isobaths of 3500, 3900, and 4500 m from GTOPO 30.

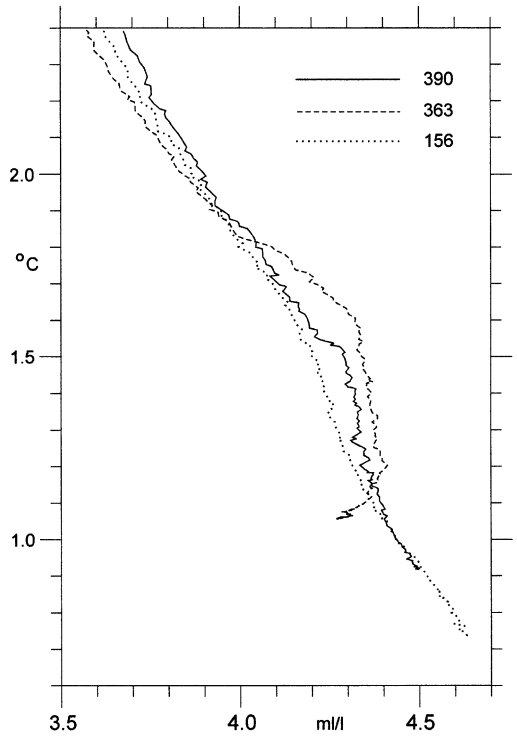

Fig. 12. Plots vs. potential temperature (°C) of dissolved-oxygen concentration (ml l^{-1}) for three stations near the 28°S passage: Sta. 363 near the western end, Sta. 390 on the central section, and Sta. 156 in the southwestern West Australian Basin. See Fig. 11 for station locations.

oxygen-rich compared to that in the southwestern West Australian Basin (Sta. 156). As stated in Section 1, the high oxygen concentration is a marker of Circumpolar Deep Water, and the values are as high as they are here because of the proximity of the mid-depth western-boundary current along the Southeast Indian Ridge that carries water directly northwestward from the Circumpolar Current (Warren, 1982; Toole and Warren, 1993). Water at comparable depths that takes the roundabout route through the Perth Basin loses this distinctive feature in transit. The contrasts are reversed below about 1.15°C (depth about 3300 m) because the saddle connecting the Southeast Indian Ridge and the Ninetyeast Ridge is too shallow to admit water of that depth directly from the south. (The GTOPO 30 bathymetry gives a sill depth between 3500 and 3600 m here.) Instead, it enters the Central Indian basin by westward overflow across the Ninetyeast Ridge, so that below 1.15°C the water at Sta. 156 is "newer" than that at Sta. 363.

Within the passage itself (Sta. 390) the water colder than 1.15°C is clearly from the West Australian Basin, and must be moving westward overall. Moreover, its temperature demonstrates that the GTOPO 30 sill depth (3500–3600 m) must be too shallow, because the lowest potential temperature on the center transect, 0.88°C on Sta. 389, is found on Sta. 156 at about 3900 m. Above 1.15°C, Sta. 390 shows the higher oxygen concentration characteristic of the Central Basin (values at Stas. 389 and 391 on the center transect are similar to those at Sta. 390). We therefore, infer that this warmer water is moving eastward, and that there is a zero-velocity surface near $\theta = 1.15$°C. This velocity profile is unlike the Denmark Strait structure seen at the two northern saddles, and is more reminiscent of the zonal jet

(Namib Col current) flowing eastward from the deep western-boundary current along the Mid-Atlantic Ridge to a deep saddle on the Walvis Ridge (Warren and Speer, 1991), although the latter includes no bottom counterflow.

In making geostrophic transport estimates for the section, since it lies wholly within the passage, we used the traditional method of Helland-Hansen (1934) to deal with the "bottom triangle" problem. Thus, we drew a profile of specific-volume anomaly for the section (Stas. 387–391) from 2000 db to the bottom, extrapolating the isanosteres into the flanks of the passage. We then constructed a curve of specific-volume anomaly vs. depth for a synthetic northern station by using Sta. 387 to its maximum pressure (2295 db), and continuing downward using the intercepts of the isanosteres with the side of the passage to the maximum pressure in the section, 4227 db at Sta. 389. We made a similar southern construction with Sta. 391 to its maximum pressure (3577 db) and isanostere-intercepts below to 4227 db. These two curves are illustrated in Fig. 13. Of course, they meet at the bottom by construction, but it is provocative that they also meet at 3400–3500 db, near the pressure at which $\theta = 1.15^{\circ}C$ (see the temperature profile, Fig. 2b, by McCarthy et al., 1997), the zero-velocity surface inferred from the water properties. Otherwise, specific-volume anomaly is everywhere greater at the northern station than at the southern one—a qualitatively different pattern from that at the 5°S and 10°S passages.

For the transport computations, we set zero velocity at 3400 db. This is also the maximum pressure at Sta. 388, so the synthetic northern station could be combined directly with Sta. 388 to calculate the transport between it and Sta. 387 (plus the channel wall below it). Similarly, the synthetic station could be paired with Sta. 389 to calculate the transport below 3400 db between Sta. 389 and the channel wall to the north. The station

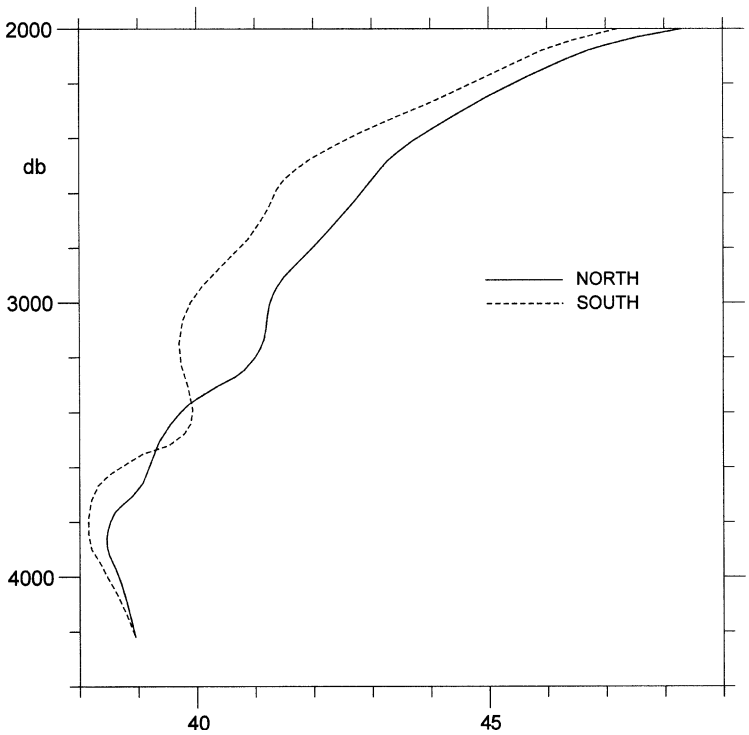

Fig. 13. Constructed curves of specific-volume anomaly (10^{-5} cm^3 g^{-1} or 10^{-8} m^3 kg^{-1} or cl ton^{-1}) vs. pressure (db) along the northern and southern flanks of the 28°S passage at the central section. See text.

pair 389–390 was integrated downward just to 4000 db, because, according to the bottom profile (McCarthy et al., 1997), that is the prevailing depth between them (Sta. 389 was occupied in a fissure). For the pair 390–391, the synthetic southern station gave the transport due to shear below 3600 db, to which we added the product of velocity calculated at 3600 db times an estimate of the cross-sectional area below (only 0.01×10^6 m^3 s^{-1}). The resulting transport estimates are 0.1×10^6 m^3 s^{-1} westward below 3400 db, and 1.7×10^6 m^3 s^{-1} eastward between 3400 and 2000 db. Moving the zero-surface by 100 db could alter the bottom-layer transport by 30%, but the upper layer transport by only a few percent; arbitrariness in isanostere intercepts might cause a reasonable uncertainty of 20% in the lower-layer value, but, again, only a few percent for the upper layer. However, the vertically averaged cross-channel difference in specific-volume anomaly below 3400 m is so small, around 2×10^{-6} cm^3 g^{-1} (Fig. 13), that possible cross-channel salinity error of 0.001 implies lower-layer transport uncertainty of 40%.

These transports are very different from those calculated by McCarthy et al. (1997): they estimated 1.0×10^6 m^3 s^{-1} westward below about 3600 m at the central section, and net *westward* flow between 3600 and 2000 m. Our construction seems more congruent with the property contrasts. If it is correct, it implies an order-of-magnitude reduction in the deep vertical diffusivity (35 cm^2 s^{-1}) calculated by McCarthy et al. (1997) for the southeastern Central Basin.

5. Discussion

The sum of these estimates of the deep overflows (below zero-velocity surfaces) into the Central Indian Basin across the Ninetyeast Ridge at the 5°S, 10°S, and 28°S saddles is 2.2×10^6 m^3 s^{-1}. As stated in Section 1, no such overflow was detected at the other deep saddle, near Lat. 3°S, in 1979. Absence of overflow there may be due to a relatively shallow sill, the depth of which, according to the GTOPO 30 bathymetry, is between 3500 and 3600 m—shallower than the zero-velocity surfaces inferred at the 5°S and 10°S saddles.

The sum for the 5°S and 10°S saddles alone (2.1×10^6 m^3 s^{-1}) is much greater than the 0.5×10^6 m^3 s^{-1} that Warren (1982) estimated from his 1979 reconnaissance section. With a zero-velocity surface at 3800 db, he obtained 0.4×10^6 m^3 s^{-1} at 10°S, but his section was higher on the ridge flank (bottom depth about 4300 m) than the WOCE one (bottom depth near 4800 m), and, as remarked in Section 2, a doubling or tripling of transport by entrainment between the two depths does not seem outlandish in consideration of the lower-limit estimates of entrainment furnished by the water-property differences. At the 5°S saddle, Warren (1982) assumed zero velocity at 4300 db and calculated an overflow of only 0.1×10^6 m^3 s^{-1}. The detailed WOCE observations show that assumption must be off by some 300 db, however, and that an assumed zero-velocity surface so deep (rather than near 4000 db) would indeed produce an insignificant transport below it (Fig. 10). This revised, enhanced estimate of the total source strength for the circulation of lower deep water in the Central Basin matches much better the independent estimate of western-boundary current transport in that layer of general magnitude 2×10^6 m^3 s^{-1} (Warren, 1982).

An unexpected finding is the large, westward transport of mid-depth water (between 2000 db and the zero-velocity surfaces) across the saddles. The net value for the three of them is 7.0×10^6 m^3 s^{-1} (westward). Given that there are segments of the Ninetyeast Ridge away from the deep saddles that are deeper than 2000 m (Fig. 1), these mid-depth flows might be merely limbs of gyres internal to the West Australian and Central Indian Basins, with compensating eastward flows at other latitudes. On the other hand, it is also conceivable that the mid-depth westward flow at the 5°S and 10°S saddles is entirely supplied by northward flow in the deep boundary current in the Perth Basin. One then asks whether that boundary current could possibly be as big as required; and, if it is, why it should be so strong at mid-depths; and further, where the inferred inflow to the Central Basin goes: upward, or returning southward at mid-depths farther to the west; and could it perhaps reach as far as the Somali Basin in the boundary current indicated along the

northeastern flank of the Mascarene Plateau (Wyrtki, 1971, p. 143), and thus complete its circuit beside Madagascar. As yet, we are unable to work out these large-scale ramifications.

Another puzzle concerns the differing characters of the mid-depth flows: westward at 10°S and 5°S, but eastward at 28°S. This difference might be related to geometry. One expects the deep western-boundary current in the Perth Basin to flow northward beside the East Indiaman Ridge (Fig. 1b) until its northern end, somewhere near Lat. 24°S, then to turn westward as a zonal jet, and to reform as a boundary-current system along the Ninetyeast Ridge near 24°S. Northward flow in this system provides the throughflows at 10°S and 5°S, which, as discussed in Section 2, density stratification causes to split in the vertical, following the Denmark Strait paradigm; but a southward branch would be needed to supply the mid-depth water in the southwestern corner of the West Australian Basin if the ridge were not broken at 28°S. Perhaps, somehow, the gap at 28°S gives preference to the boundary current along the Southeast Indian Ridge as the mid-depth source for this corner region, rather than the presumed zonal flow to the north.

The GTOPO 30 bathymetry places the sill for the junction between the Southeast Indian and Ninetyeast Ridges at 33°10′S, 85°20′E, with a depth between 3500 and 3600 m. If this is true, and if the lower limit of the water entering the Central Basin directly from the south is something like 3600 m, then that also might be the maximum depth for eastward flow through the 28°S passage, potentially leaving a small vertical interval below it for westward flow of denser water from the West Australian Basin. The mid-depth eastward flow itself, turning northward as a western-boundary current along the Ninetyeast Ridge, could return to the western Central Indian Basin in the mid-depth westward flow at the 10°S saddle. Indeed, such a scheme in which water from a western-boundary current strikes eastward in a zonal jet to a gap in a ridge, proceeds as a boundary current along the eastern side of the ridge, encounters another gap, and returns to the original boundary current in a westward jet at the gap latitude matches some of Pedlosky's (2001) recent ideas about flow through ridges with narrow gaps. Again, we cannot proceed farther.

We suggested uncertainties in the transport estimates due to salinity error, perturbation of zero-velocity surfaces, and treatments of "bottom triangles". It would be pedantic, however, to sum these as "error bars" for the estimates, because, as with all such thermal-wind calculations, the prime question is the credibility of the basic zero-velocity surfaces, which cannot usefully be quantified. We constructed our surfaces from water-property evidence concerning flow directions, which other investigators might interpret differently, and for that matter it is not unknown for direct current measurements to defy the apparent demands of property fields. Readers will have to make their own judgments of the firmness of our estimates.

A different question is how representative the observed thermal-wind fields are of the long-term mean flows. Without repeated hydrographic stations or current-meter time series we cannot say. However, steady oceanic sill overflows are sometimes predicted using a rotating hydraulic-control model (Whitehead, 1998). Density–depth curves from WOCE Sections I9N (nominal Long. 95°W) and I8N (nominal Long. 80°W) around the sill latitudes at 5°S and 10°S were incorporated into this model. It uses this information from basins on either side of a sill, together with the sill depth, width, and latitude to estimate a maximum transport through the sill. For both sills this transport estimate was 3×10^6 m^3 s^{-1}, but with order one uncertainties owing to uncertainties in sill depths and the likelihood of temporal variations in isopycnal depth. These estimates are larger than those reported here, a typical result when comparing the maximum rotating-hydraulic-control-model transport estimates to direct measurements (Whitehead, 1998). What the model does suggest is that a sufficient hydraulic head exists to drive relatively steady overflows; but it is not so sure that hydraulic control pertains to these overflows, or, if it does, that the expectation of maximum (i.e. steady) transport is justified.

In any case, swift flows through narrow passages are commonly dominated by their means. Thus, current records in the cold outflow through the Faroe Bank Channel (from the Norwegian

Basin to the Iceland Basin) had standard deviations roughly 17% of the means (Saunders, 1990); Hogg et al. (1982) observed the standard deviation of the volume transport of Antarctic Bottom Water through the Vema Channel (connecting the Argentine to the Brazil Basin) to be 30% of the mean; and a dense array of current meters in the Samoan Passage (between the deep South and North Pacific) measured the standard deviation of the northward transport of bottom water as 25% of the mean (Rudnick, 1997). An exception to this general rule is the flow through the Charlie–Gibbs Fracture Zone (joining the deep subpolar eastern and western North Atlantic through the Mid-Atlantic Ridge), which is dominated by bursts of westward current, producing a standard deviation of the transport record some 125% of the mean (Saunders, 1994).

Nevertheless, we likened the 5°S and 10°S flows to that through the Denmark Strait. In the bulk of the dense, descending part of that current, Dickson and Brown (1994) measured the mean kinetic energies to be several times the eddy kinetic energies. We expect that the Ninetyeast Ridge overflows also will be found to be in the group of relatively low variability, so that our transport estimates, if reliable snapshots, ought to be fairly representative of the means.

Acknowledgements

This research is part of the WOCE Hydrographic Program in the Indian Ocean, and was funded by various grants from the US National Science Foundation, the National Oceanic and Atmospheric Administration, and the National Atmospheric and Space Administration. It is Contribution Number 10,316 from the Woods Hole Oceanographic Institution and Contribution Number 2238 from the Pacific Marine Environmental Laboratory.

References

Dickson, R.R., Brown, J., 1994. The production of North Atlantic Deep Water: Sources, rates and pathways. Journal of Geophysical Research 99, 12319–12341.

Fisher, R.L., Jantsch, M.Z., Comer, R.L (Scientific coordinators), 1982. General Bathymetric Chart of the Oceans (GEBCO), Sheet 5.09. Canadian Hydrographic Service, Ottawa.

Gordon, L.I., Jennings Jr., J.C., Ross, A.A., Krest, J.M., 1994. A suggested protocol for continuous flow automated analysis of seawater nutrients (phosphate, nitrate, nitrite and silicic acid) in the WOCE Hydrographic Program and the Joint Global Ocean Fluxes Study. WOCE Operations Manual, WOCE Report No. 68/91. Revision 1.

Helland-Hansen, Bj., 1934. The Sognefjord section. Oceanographic observations in the northernmost part of the North Sea and the southern part of the Norwegian Sea. In: Daniel, R.J. (Ed.), James Johnstone Memorial Volume. University Press of Liverpool, Liverpool, pp. 257–274.

Hogg, N., Biscaye, P., Gardner, W., Schmitz Jr., W.J., 1982. On the transport and modification of Antarctic Bottom Water in the Vema Channel. Journal of Marine Research 40 (Suppl.), 231–263.

Mantyla, A.W., Reid, J.L., 1995. On the origins of deep and bottom waters of the Indian Ocean. Journal of Geophysical Research 100, 2417–2439.

McCarthy, M.C., Talley, L.D., Baringer, M.O., 1997. Deep upwelling and diffusivity in the southern Central Indian Basin. Geophysical Research Letters 24, 2801–2804.

Pedlosky, J., 2001. Steady baroclinic flow through ridges with narrow gaps. Journal of Physical Oceanography 31, 2418–2440.

Price, J.M., Baringer, M.O., 1994. Outflows and deep water production by marginal seas. Progress in Oceanography 33, 161–200.

Rudnick, D., 1997. Direct velocity measurements in the Samoan Passage. Journal of Geophysical Research 102, 3293–3302.

Saunders, P.M., 1990. Cold outflow from the Faroe Bank Channel. Journal of Physical Oceanography 20, 29–43.

Saunders, P.M., 1994. The flux of overflow water through the Charlie–Gibbs Fracture Zone. Journal of Geophysical Research 99, 12343–12355.

Smith, W.H.F., Sandwell, D.T., 1997. Global seafloor topography from satellite altimetry and ship depth soundings. Science 277, 1956–1962.

Spall, M.A., Price, J.F., 1998. Mesoscale variability in Denmark Strait: the PV outflow hypothesis. Journal of Physical Oceanography 28, 1598–1623.

Swallow, J.C., Worthington, L.V., 1969. Deep currents in the Labrador Sea. Deep-Sea Research 16, 77–84.

Talley, L.D., Baringer, M.O., 1997. Preliminary results from WOCE hydrographic sections at 80°E and 32°S in the Central Indian Ocean. Geophysical Research Letters 24, 2789–2792.

Toole, J.M., Warren, B.A., 1993. A hydrographic section across the subtropical South Indian Ocean. Deep-Sea Research 40, 1973–2019.

Warren, B.A., 1981. Transindian hydrographic section at Lat. 18°S: property distributions and circulation in the South Indian Ocean. Deep-Sea Research 28A, 759–788.

Warren, B.A., 1982. The deep water of the Central Indian Basin. Journal of Marine Research 40 (Suppl.), 823–860.

Warren, B.A., Owens, W.B., 1988. Deep currents in the central subarctic Pacific Ocean. Journal of Physical Oceanography 18, 529–551.

Warren, B.A., Speer, K.G., 1991. Deep circulation in the eastern South Atlantic Ocean. Deep-Sea Research 38 (Suppl. IA), S281–S322.

Whitehead, J.A., 1998. Topographic control of oceanic flows in deep passages and straits. Reviews of Geophysics 36, 423–440.

Wyrtki, K., 1971. Oceanographic Atlas of the International Indian Ocean Expedition. National Science Foundation, Washington, DC, 531 + xi pp.